Structural Characterization of Single-Walled Carbon Nanotube Bundles by Experiment and Molecular Simulation

Sandeep Agnihotri,[†] José P. B. Mota,*[,‡] Massoud Rostam-Abadi,*[,†,§] and Mark J. Rood[†]

Department of Civil and Environmental Engineering, University of Illinois, Urbana-Champaign, 205 N. Mathews Avenue, Urbana, Illinois 61801-2352, Requimte/CQFB, Departamento de Química, Faculdade de Ciências e Tecnologia, Universidade Nova de Lisboa, 2829-516 Caparica, Portugal, and Illinois State Geological Survey, 615 E. Peabody Drive, Champaign, Illinois 61820

Received September 20, 2004. In Final Form: November 12, 2004

A procedure, combining molecular simulation, Raman spectroscopy, and standard nitrogen adsorption, is developed for structural characterization of single-walled carbon nanotube (SWNT) samples. Grand canonical Monte Carlo simulations of nitrogen adsorption are performed on the external and internal adsorption sites of homogeneous arrays of SWNTs of diameters previously determined by Raman spectroscopy of the sample. The results show the importance of the peripheral grooves of a nanotube bundle at low relative pressure and the insensitivity of nanotube diameter toward adsorption on the external surface of the bundle at higher pressures. Simulations also reveal that samples containing thin nanotubes have less internal adsorption capacity that saturates at lower pressure than those comprising large diameter nanotubes. The fraction of open-ended nanotubes in a sample can be estimated by scaling the simulated internal adsorption inside nanotubes to obtain a near perfect fit between simulated and experimental isotherms. This procedure allows extrapolation of adsorption properties to conditions in which all nanotubes in the sample are open-ended.

1. Introduction

Single-walled carbon nanotubes (SWNTs) are receiving much attention due to their remarkable physical and electronic properties.[1] The hollow one-dimensional and one-atom-thick structure of SWNTs is especially attractive for adsorption-related applications. The use of nanotubes for developing sensors of pollutant gases,[2] storage of alternative fuels,[3] and removal of hazardous pollutants from gas streams[4,5] is being studied extensively, for which the characterization of their adsorption properties is important.

Studies related to the adsorption of various gases on carbon nanotubes have explored different aspects of nanotube−adsorbate interactions. Molecular simulation of nitrogen adsorption on arrays of close-ended and open-ended SWNTs has shown that high adsorption capacities can be obtained for narrow SWNTs (6 Å) that are widely (30 Å) spaced.[6] In such structures, adsorption on the outer surface of SWNTs dominates, which would render the opening of nanotubes unnecessary. The adsorption surface area of such SWNTs can be as high as 3000 m^2/g, which remains the highest theoretically calculated surface area of nanotubes. An experimental investigation of N_2 adsorption on as-produced HiPco SWNTs has reported a unique purification process that exfoliates SWNT bundles into individual nanotubes to yield a surface area as high as 1587 m^2/g.[7] Common oxidative purification of as-produced HiPco SWNTs is now known to change the characteristics of N_2 adsorption isotherms from type II to type IV.[8] Heating as-produced SWNTs in air at 350 °C has demonstrated a 2-fold increase in the N_2 and O_2 adsorption capacities, probably due to the opening of nanotubes.[9] The isosteric heat of adsorption of N_2 on close-ended SWNTs is noted to be a function of surface coverage due to the presence of multiple adsorption sites on a bundle.[10] Density functional theory calculations have reported that O_2 molecules dissociatively chemisorb on nanotubes[11] and gas molecules (N_2, O_2, NH_3, NO_2, H_2O, CO_2, etc.) adsorb weakly on SWNT bundles with a small charge transfer that can alter the electrical properties of nanotubes.[12,13] Other important studies on nanotube−gas interactions have revealed two distinct types of

* To whom correspondence should be addressed. Phone: (351) 21-2948300, ext. 10961 (J.P.B.M.); (217) 244-4977 (M.R.A.). Fax: (351) 21-2948385 (J.P.B.M.); (217) 333-8566 (M.R.A.). E-mail: pmota@dq.fct.unl.pt (J.P.B.M.); massoud@isgs.uiuc.edu (M.R.A.).

[†] University of Illinois.

[‡] Universidade Nova de Lisboa.

[§] Illinois State Geological Survey.

(1) Dresselhaus, M. S.; Dresselhaus, G.; Avouris, P. *Carbon nanotubes: synthesis, structure, properties and applications*; Topics in Applied Physics; Springer: New York, 2000; Vol. 80.

(2) Kong, J.; Franklin, N. R.; Zhou, C.; Chapline, M. G. *Science* **2000**, *287*, 622.

(3) Liu, C.; Fan, Y. Y.; Liu, M.; Cong, H. T.; Cheng, H. M.; Dresselhaus, M. S. *Science* **1999**, *286*, 1127.

(4) Long, R. Q.; Yang, R. T. *J. Am. Chem. Soc.* **2001**, *123*, 2058.

(5) Long, R. Q.; Yang, R. T. *Ind. Eng. Chem. Res.* **2001**, *40*, 4288.

(6) Yin, Y. F.; Mays T.; McEnanaey, B. *Langmuir* **1999**, *15*, 8714.

(7) Cinke, M.; Li, J.; Chen, B.; Cassell, A.; Delzeit, L.; Han, J. *Chem. Phys. Lett.* **2002**, *365*, 69.

(8) Yang, C. M.; Kaneko, K.; Yudasaka M.; Iijima S. *Nano Lett.* **2002**, *2*, 385.

(9) Fujiwara, A.; Ishji, K.; Suematsu, H.; Kataura, H.; et al. *Chem. Phys. Lett.* **2001**, *336*, 205.

(10) Yoo, D. H.; Rue, G. H.; Hwang, Y. H.; Kim, H. K. *J. Phys. Chem. B* **2002**, *106*, 3371.

(11) Zhu, X. Y.; Lee, S. M.; Lee, Y. H.; Frauenheim, T. *Phys. Rev. Lett.* **2000**, *85*, 2757.

(12) Zhao, J.; Buldum, A.; Han, J.; Lu, J. P. *Nanotechnology* **2002**, *13*, 195.

(13) Chang, H.; Lee, J. D.; Lee, S. M.; Lee, Y. H. *Appl. Phys. Lett.* **2001**, *79*, 3863.

10.1021/la047662c CCC: $30.25
Published on Web 01/07/2005

adsorption surfaces on SWNTs,[14] capillary condensation of CH_4 inside open-ended nanotubes,[15] stronger interaction of Xe, Ne, and CH_4 with nanotubes than with graphite,[16] displacement of CO_2 by Xe in SWNT bundles as observed by infrared spectroscopy and molecular simulations,[17] and calculation of Ar and Ne diffusivities in homogeneous arrays of SWNTs.[18]

In general, the reported Brunauer−Emmett−Teller (BET) surface area of SWNTs ranges from 150 to 1587 m^2/g and depends on the adsorbate gas used for analysis and the specific structure and composition of the sample.[7] In most of these studies, the nanotubes were subjected to oxidative purification processes that not only enhanced the purity of the sample but also opened the nanotube ends.[7,9] However, a precise quantification of open-ended nanotubes has not been completely established[7] and the assumption that all nanotubes are open is usually made. To the best of our knowledge, only Du et al.[19] have described a rudimentary procedure for determining the relative amount of open-ended SWNTs in tested samples. These authors used pore-size distributions to determine that as-produced HiPco SWNTs[20,21] contain as much as 40% open-ended nanotubes; this percentage can be increased using a suitable purification process.

The overall adsorption on SWNTs is a contribution from various adsorption sites. Due to strong van der Waals interactions, SWNTs adhere to each other and form bundles or ropes and, thus, the adsorption sites are defined for the entire bundle as opposed to an individual nanotube.[16,19,22] There are four possible sites for adsorption: the hollow interior of nanotubes, the interstitial channels between the nanotubes, the grooves present on the periphery of a nanotube bundle, and the exterior surface of the outermost nanotubes (Figure 1).[12]

Due to the structure of the bundles, the intratube space is the most easily visualized adsorption site, potentially providing a large volume for adsorption and gas storage. However, unlike other sites which are all available for adsorption on open- and close-ended nanotubes, the intratube volume is accessible only for open-ended nanotubes. The knowledge of the fraction of open-ended nanotubes in a sample is, thus, essential to determine the amount of adsorption that occurs inside a nanotube bundle.

In this study, molecular simulation of nitrogen adsorption in SWNT bundles is carried out and the results are compared to those of an experimental study.[23] The nitrogen adsorption capacity of bundles of open-ended nanotubes is determined by grand canonical Monte Carlo (GCMC) simulation. The nanotube diameters selected for calculation are the ones determined by Raman spectroscopy of the samples considered in this study.[23] The simulations show that N_2 adsorption on the external grooves occurs at relative vapor pressures as low as 10^{-6} and that the total adsorption on the external adsorption sites (i.e., grooves and external surface) is weakly dependent on nanotube diameter. Adsorption in the interstitial channels of homogeneous bundles can occur only for large tube diameters. The total adsorption in the internal sites of a homogeneous bundle, averaged over all nanotube diameters according to their weight fraction in the sample, can be adjusted by a scaling factor to give a near perfect fit between calculated and experimental values of adsorption isotherm, surface area, and pore volume. This factor is interpreted as an estimate of the weight fraction of open-ended nanotubes present in the sample.

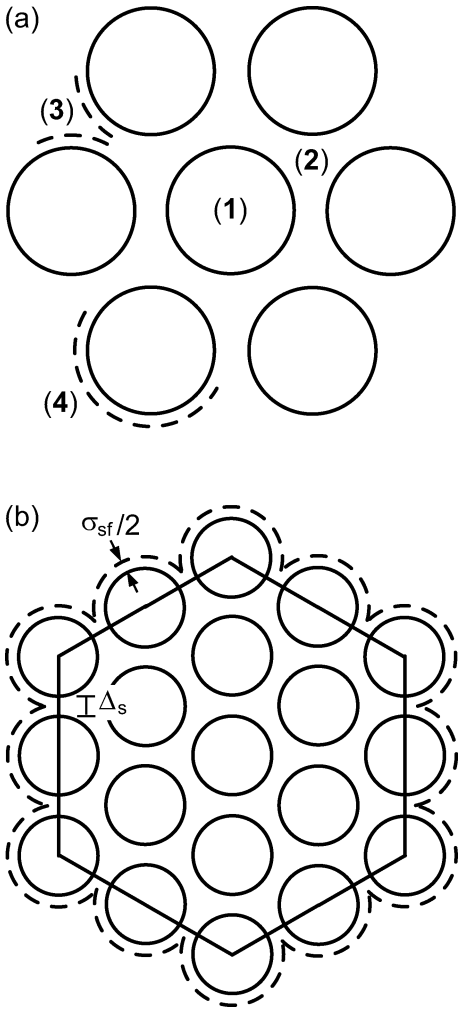

Figure 1. (a) Four different adsorption sites on a homogeneous bundle of open-ended SWNTs: (1) internal (endohedral), (2) interstitial channels, (3) external groove sites, and (4) external surface. (b) We define the external surface area of a bundle as the area of the plane boundaries of the prism with vertices on the center of the outermost shell of nanotubes (solid line). This is an unambiguous definition of external surface that is independent of sorbate size. It can be converted to that represented by the dashed line using the conversion formula $S'_p = S_p(\pi/2 - \theta)/\cos\theta$, where $\cos\theta = (D + \Delta_s)/(D + \sigma_{sf})$, D is the tube diameter, $\Delta_s = 3.4$ Å is the intertube distance, and σ_{sf} is the collision diameter for sorbate−carbon interaction.

2. Experiments, Simulation, and Analytical Methods

GCMC simulations were performed to predict the experimental nitrogen adsorption capacities of two purified nanotube samples containing open-ended SWNTs. The experimental details are provided elsewhere,[23] and only a brief description of the results is presented here.

(14) Muris, M.; Dufau, N.; Biefait, M.; Dupont-Povlovsky, N. *Langmuir* **2000**, *16*, 7019.
(15) Mackie, E. B.; Wolfson, R. A.; Arnold, L. M.; Lafdi, K.; Migone, A. D. *Langmuir* **1997**, *13*, 7197.
(16) Talapatra, S.; Zambano, A. Z.; Weber, S. E.; Migone, A. D. *Phys. Rev. Lett.* **2000**, *85*, 138.
(17) Matranga, C.; Chen, L.; Bockrath, B.; Johnson, J. K. *Phys. Rev. B* **2004**, *70*, 165416.
(18) Ackerman, D. M.; Skoulidas, A. I.; Sholl, D. S.; Johnson, J. K. *Mol. Simul.* **2003**, *29*, 677.
(19) Du, W.; Wilson, L.; Ripmeester, J.; Dutrisac, R.; Simard, B.; Denommee, S. *Nano Lett.* **2002**, *2*, 343.
(20) Nikolaev, P.; Bronikowski, M. J.; Bradley, R. K.; Rohmund, F.; et al. *Chem. Phys. Lett.* **1999**, *313*, 91.
(21) Bronikowski, M. J.; Willis, P. A.; Colbert, D. T.; Smith, K. A.; Smalley, R. E. *J. Vac. Sci. Technol., A* **2001**, *19*, 1800.
(22) Shi, W.; Johnson, J. K. *Phys. Rev. Lett.* **2003**, *91*, 015504.
(23) Agnihotri, S.; Rostam-Abadi, M.; Rood, M. J. *Carbon* **2004**, *42*, 2699.

Table 1. Composition of SWNT Samples

sample	wt %[a] SWNTs	wt %[a] impurities	diameter, D^b (Å)	weight fraction, $w_D{}^b$
EA95	95−98	3−5	11.5	0.15
			14.0	0.34
			15.2	0.51
CVD80	≈80	≈20	09.0	0.42
			10.2	0.21
			10.7	0.17
			11.1	0.11
			11.8	0.10

[a] Manufacturer specified information. [b] Determined by Raman analysis.

Table 2. Lennard-Jones Potential Parameters

site−site	ϵ/k_B (K)	σ (Å)
C-C	028.0	3.400
N_2-N_2	100.4	3.609

The SWNT samples tested were manufactured by the electric-arc and HiPco chemical vapor deposition (CVD) methods[20,21] and contained 95−98 wt % (EA95) and ≈80 wt % (CVD80) SWNTs, respectively. The nanotube diameters and their weight fraction in each sample were determined by Raman spectroscopy (Table 1). Sample EA95 contains mainly three different-sized nanotubes, with the majority of them being 15.2 Å wide. Sample CVD80, on the other hand, is more heterogeneous. The nanotubes in this sample have mainly five different sizes, with most of them being 9.0 Å in diameter.

The nitrogen adsorption isotherm ($10^{-6} < P/P_0 < 0.99$), BET surface area ($0.03 < P/P_0 < 0.3$), and total and micropore volumes of each sample were determined experimentally by standard nitrogen adsorption (77 K) on a Micromeritics ASAP 2010 surface area analyzer. The samples analyzed were sufficiently aged (older than 7 months) to minimize the impact of aging.[23]

In the molecular simulations reported here, the nitrogen molecules are treated as structureless spherical particles interacting via dispersive forces only. Although the N_2 molecule has a quadrupole moment, it does not significantly change the simulated adsorption isotherm at 77 K. The interaction between N_2 molecules is modeled by the 12-6 Lennard-Jones potential

$$u_{ij}(r) = 4\epsilon_{ij}[(\sigma_{ij}/r)^{12} - (\sigma_{ij}/r)^6] \quad (1)$$

(r is the intermolecular distance), as is the interaction between the carbon atoms of a nanotube and each N_2 molecule. The well depths, ϵ_i/k_B, where k_B is the Boltzmann constant, and collision diameters, σ_i, used are listed in Table 2. The N_2 parameters were obtained by fitting the simulated vapor−liquid coexistence curve to experimental data using the procedure of Errington and Panagiotopoulos.[24] The cross terms were obtained using the standard Lorenz−Berthelot combining rules: $\epsilon_{ij} = (\epsilon_i\epsilon_j)^{1/2}$ and $\sigma_{ij} = (\sigma_i + \sigma_j)/2$.

To simulate nitrogen adsorption on a real sample, a simulation box containing a heterogeneous distribution of nanocylinders would be the most appropriate structural arrangement of nanotubes. However, making heterogeneous nanotube bundles[22] that closely resemble the bundle size and the diameter distribution of the experimental samples is a very time-consuming task; thus, an alternative methodology was employed.

(24) Errington, J. R.; Panagiotopoulos, A. Z. *J. Chem. Phys.* **1998**, *109*, 1093.

Simulations were performed on homogeneous arrays of SWNTs of diameters listed in Table 1. The positions of the individual carbon atoms in a nanotube are assumed unimportant at the temperatures of interest in this study; that is, each nanotube in the bundle is considered to be a smooth, structureless nanocylinder. At very low temperatures, corrugation effects would become important. An effective potential is developed by integrating the $C-N_2$ potential over the positions of all carbon atoms in a tube of infinite length:

$$U_{sf}(\delta) = \frac{2D}{a_c}\int_0^{+\infty}\int_0^{\pi} u_{sf}(r)\, d\theta\, dz,$$
$$r^2 = (D/2)^2 + \delta^2 + z^2 - \delta D\cos\theta \quad (2)$$

where U_{sf} is the interaction potential between a nitrogen molecule at the nearest distance, δ, from the central axis of a nanotube of diameter D, z is the distance along the tube axis (considered infinite), θ is the radial angle, and $a = 2.6185$ Å^2 is the surface area per carbon atom of the tube. By integrating over z and θ, eq 2 is reduced to a one-dimensional potential which depends on δ only.

The multidimensioned integral in eq 2 was numerically evaluated using subroutine QB01 of the Harwell FORTRAN library. Simpson's rule was selected as the integration method with a prescribed relative accuracy set to 10^{-5}. To speed up the calculation of U_{sf}, eq 2 was tabulated on a one-dimensional grid. For intratube values of δ in the range $[0, D/2]$, the potential was tabulated on a grid with 31 knots equally spaced in δ^2; for outertube values of δ in the range $[D/2, 3.5D]$, the grid employed 56 knots equally spaced in $1/\delta^2$. The potential was truncated at $3.5D$. During the simulations, U_{sf} was reconstructed from the tabulated information using cubic Hermite polynomial interpolation.

The simulations were carried out in two stages: adsorption on the external surface of the nanotube bundle (i.e., grooves and external surface) and adsorption inside the bundle (i.e., intratube and interstitial channels). The intertube distance for all simulations was kept fixed at $\Delta_s = 3.4$ Å. Figure 2 shows the cross section, perpendicular to the tube axis, of the unit simulation boxes employed in this work. The cross-sectional shape, identified by the gray area, depends on the region of the nanotube bundle being probed. The faces of each simulation box implement periodic boundary conditions, except for the top face of the box in Figure 2a, which is a reflecting wall, and the bottom one of the same box, which is blocked by the outermost shell of nanotubes in the bundle. The actual length of the simulation box was a function of the imposed sorbate pressure to keep an average number of molecules in the box greater than 50.

When simulating adsorption on the external surface of the bundle, a molecule is mapped onto the hatched area of Figure 2a and interacts with the five nearest nanotubes (three on the outermost shell and two on the second shell). Including farther nanotubes has a minimum impact on the total solid−fluid interaction potential. Notice that the nanotubes are not part of the simulation box and, therefore, molecules are not allowed to adsorb inside of them. We also explored the alternative of making the outermost shell of nanotubes accessible for internal adsorption and then correcting the final results by subtracting the average intratube adsorption from the total number of adsorbed molecules. The comparison of both methods showed that the external adsorption is not affected by intratube adsorption on the outermost shell.

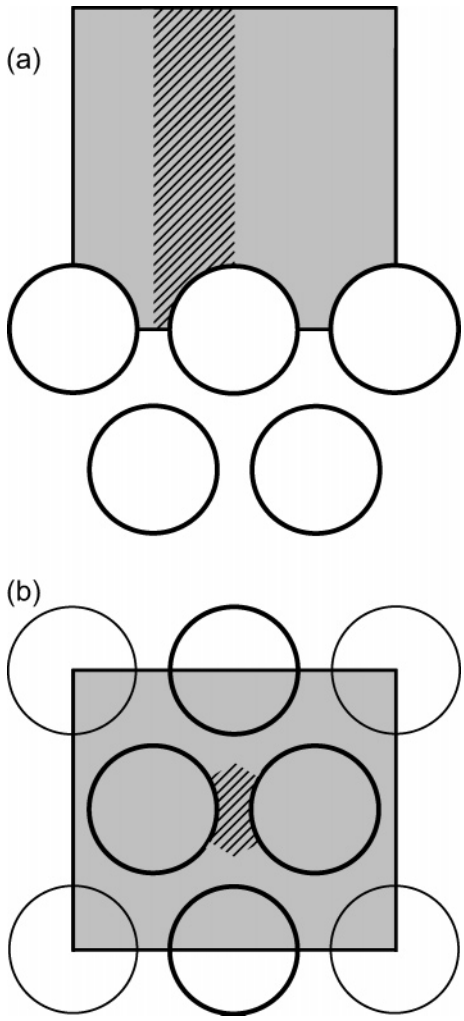

Figure 2. Cross section of the unit simulation box for GCMC study of nitrogen adsorption onto different adsorption sites of a bundle of open-ended SWNTs: (a) the external groove sites and external surface; (b) the internal (endohedral) and interstitial channels. The gray area represents the effective volume probed during the simulation. In each plot, the nanotubes printed in thicker lines are the contributing ones for the solid−fluid interaction potential of an adsorbate molecule placed in the hatched area.

Figure 2b shows the cross section of the unit simulation box employed to study internal and interstitial adsorption. To calculate the solid−fluid interaction potential of a molecule located inside a nanotube of the bundle, it suffices to sum over the interactions of the molecule with the confining tube and the six nearest neighbors. The corrugation effect of the neighboring tubes is very small and, for practical purposes, does not affect the cylindrical symmetry of the total interaction potential. The net effect is that the potential curve for intratube adsorption in the bundle has the same shape as that for an isolated tube, though the well depth is deeper. We also take into account N_2 adsorption in the interstitial regions (where three tubes meet). A molecule in one of such regions can be mapped onto the hatched area shown in Figure 2b. The solid−fluid potential there is calculated by summing over the interactions of the molecule and the four nearest tubes, which are plotted by thicker lines in Figure 2b. It was observed that including farther nanotubes does not change appreciably the interaction potential. Unlike the potential inside the tube, the solid−fluid interaction potential in the interstitial region is not cylindrically symmetric.

The GCMC simulations were carried out using established procedures.[25] In normal GCMC, insertions are attempted uniformly throughout the volume of the simulation box. For nanotube bundles, however, it is known a priori that much of this volume is filled by carbon atoms of the nanotubes and is inaccessible to sorbate molecules. Furthermore, not all portions of the accessible space are equally favorable; preferred regions exist in which sorbate molecules are localized. This information can be incorporated into a GCMC simulation if the insertions are not attempted randomly throughout the volume. This was achieved in this work by using configurational-bias techniques.[26−29] Due to the bias introduced into the Monte Carlo insertion moves, the acceptance rules for insertions and deletions must be altered to ensure that microscopic reversibility is satisfied and that the ensemble is still correctly sampled. The method has been described in detail elsewhere.[25]

In this work, one of the simplest biased GCMC schemes was employed. The method is based on one of the techniques proposed by Snurr et al.[30] in their simulation work of the adsorption of aromatic hydrocarbons in silicalite. An insertion is performed as follows. A number, n_{trial}, of trial positions are randomly chosen throughout the simulation volume, V. For each point $j = 1, \ldots, n_{\text{trial}}$, we calculate the solid−fluid potential energy, $U_{\text{sf}}^{(j)}$, due to the interaction between a sorbate molecule placed at that point and the potential field of the nanotube array, as well as the corresponding Boltzmann factor, $\exp[-\beta U_{\text{sf}}^{(j)}]$, where $\beta = (k_B T)^{-1}$ and T is the system temperature. Out of the n_{trial} trial positions, one, denoted by i, is selected with a probability of

$$\mathscr{P}^{(i)} = W_{\text{sf}}^{-1} \exp[-\beta U_{\text{sf}}^{(i)}], \quad W_{\text{sf}} = \sum_{j=1}^{n_{\text{trial}}} \exp[-\beta U_{\text{sf}}^{(j)}] \qquad (3)$$

The insertion of the molecule at the selected trial position is accepted with a probability of

$$\text{acc}(N \rightarrow N+1) = \min\left\{1, \frac{W_{\text{sf}}}{n_{\text{trial}}} \frac{fV}{N+1} \beta \exp(-\beta \Delta U_{\text{ff}})\right\} \qquad (4)$$

where N is the number of sorbate molecules present before the attempted insertion, f is the imposed vapor fugacity, and $\Delta U_{\text{ff}} = U_{\text{ff}}(N+1) - U_{\text{ff}}(N)$ is the change in the total sorbate−sorbate contribution to the potential energy of the system due to the insertion.

A deletion is performed by randomly choosing a molecule and calculating the potential energy, $U_{\text{sf}}^{(1)}$, due to its interaction with the nanotube bundle. $n_{\text{trial}} - 1$ trial positions are randomly chosen throughout the simulation volume, and $U_{\text{sf}}^{(j)}$ is computed for each trial point $j = 2, \ldots, n_{\text{trial}}$, as well as the quantity

(25) Frenkel, D.; Smit, B. *Understanding Molecular Simulation*; Academic Press: London, 1996.
(26) Siepmann, J. I. *Mol. Phys.* **1990**, *70*, 1145.
(27) Siepmann, J. I.; Frenkel, D. *Mol. Phys.* **1992**, *75*, 59.
(28) Frenkel, D.; Mooij, G. C. A. M.; Smit, B. *J. Phys.: Condens. Matter* **1992**, *4*, 3053.
(29) de Pablo, J. J.; Laso, M.; Sutter, U. W. *J. Chem. Phys.* **1992**, *96*, 2395.
(30) Snurr, R. Q.; Bell, A. T.; Theodorou, D. N. *J. Phys. Chem.* **1993**, *97*, 13742.

$$W_{sf} = \sum_{j=1}^{n_{trial}} \exp[-\beta U_{sf}^{(j)}] \quad (5)$$

The deletion attempt is accepted with a probability of

$$\mathrm{acc}(N \rightarrow N-1) = \min\left\{1, \frac{n_{trial}}{W_{sf}} \frac{N}{fV} \beta^{-1} \exp(-\beta \Delta U_{ff})\right\} \quad (6)$$

where $\Delta U_{ff} = U_{ff}(N-1) - U_{ff}(N)$ is the change in the total sorbate−sorbate contribution to the potential energy of the system due to the molecule deletion.

Each simulation run was equilibrated for 10^4 Monte Carlo cycles, where each cycle consists of N attempts to translate a randomly selected molecule and $\max\{30, 0.3N\}$ attempts to create or delete a molecule with $n_{trial} = 100$. Here, N is the number of molecules in the box at the beginning of each cycle. The production period consisted of 3×10^4 Monte Carlo cycles. The maximum displacement for translation in the simulation box was adjusted during the equilibration phase to give a 50% acceptance rate. Standard deviations of the ensemble averages were computed by breaking the production run into five blocks.

For a given bundle with tube diameter D and specified relative pressure P/P_0, the excess adsorption in the two regions of Figure 2 is computed as

$$q^{s}_{sim,D} = (\langle N \rangle - \rho_g V)/A \quad (7)$$

$$q^{i}_{sim,D} = (\langle N \rangle - \rho_g V)/n \quad (8)$$

where $q^{s}_{sim,D}$ and $q^{i}_{sim,D}$ denote, respectively, the simulated amounts adsorbed on the external surface and inside the bundle, $\langle N \rangle$ is the ensemble average of the number of sorbate molecules in the simulation box, ρ_g is the corresponding vapor density at the imposed temperature and pressure conditions, V is the simulation volume, A is the area of the bottom face of the smallest parallelepiped that encloses the box of Figure 2a, and n_c is the number of carbon atoms in the box of Figure 2b. Notice that $q^{s}_{sim,D}$ is in accordance with our definition of external surface area, as described in Figure 2a. In this work, the values of $q^{s}_{sim,D}$ and $q^{i}_{sim,D}$ are reported in units of cm^3 [STP]/m^2 and cm^3 [STP]/g, respectively.

Once the external and internal adsorption capacities of homogeneous nanotube bundles have been determined by simulation, the overall adsorption, q_{sim}, for a SWNT sample is estimated by averaging the adsorption contributions from bundles of nanotubes sizes relevant to the sample:

$$q_{sim}(P/P_0) = S_p q^{s}_{sim}(P/P_0) + (1-\eta) q^{i}_{sim}(P/P_0) \quad (9)$$

$$\{q^{s}_{sim}, q^{i}_{sim}\}(P/P_0) = \sum_{D=\text{sample}} w_D \{q^{s}_{sim,D}, q^{i}_{sim,D}\}(P/P_0) \quad (10)$$

where w_D is the weight fraction of nanotubes of diameter D in the sample (Table 1), 100η is the weight percent of impurities in the sample (Table 1), and S_p is the external surface area of the bundles in the sample (Figure 1b). Since eq 9 assumes that all nanotubes are open-ended, $q_{sim}(P/P_0)$ is an upper limit on the total amount adsorbed on the sample at the specified relative pressure. Note that the small contribution of impurities to the external surface area of the sample is lumped into the value of q^{s}_{sim}.

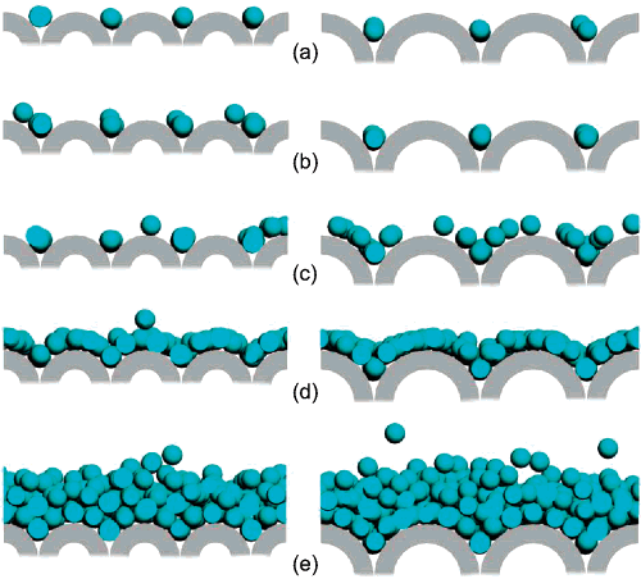

Figure 3. Snapshots of the simulation box for nitrogen adsorption at 77 K on the external surface of homogenous SWNT bundles of tube diameter $D = 9.0$ Å (left) and $D = 15.2$ Å (right): (a) $P/P_0 = 10^{-6}$; (b) 10^{-4}; (c) 10^{-3}; (d) 10^{-2}; (e) 0.9.

3. Results and Discussion

3.1. External Adsorption. The simulations show that the external grooves of a nanotube bundle play an important role in adsorption on the external surface of the bundle (henceforth, referred to as external adsorption) at low relative vapor pressures. Adsorption in these sites is observed at pressures as low as $P/P_0 = 10^{-6}$ and continues until they are saturated at about $P/P_0 = 10^{-4}$. Other authors[19,23] have also suggested the possibility of adsorption in external grooves. However, their results were based on speculations to justify the peaks observed in the 4−5 Å region of pore-size distribution of their samples.[23] The results presented here support the hypothesis that such peaks most likely arise from the adsorption on the external grooves of a nanotube bundle, although the adsorption in larger interstitial channels,[22] arising from the heterogeneity introduced by the nonuniform tube size distribution, cannot be ruled out.

Increasing the vapor pressure above $P/P_0 = 10^{-4}$ results in adsorption on the curved surface of the outer nanotubes. At $P/P_0 \approx 10^{-3}$, partial coverage of the external surface is observed. Further increase in vapor pressure until $P/P_0 = 10^{-2}$ results in complete monolayer formation following which adsorption proceeds rapidly with increasing vapor pressure. The mechanism of nitrogen adsorption on the external surface of nanotubes is illustrated in Figure 3. It is also observed that the trend in external adsorption is independent of nanotube size. Adsorption on an array of 15.2 Å diameter nanotubes takes place in more or less the same way as that on a 9.0 Å wide nanotube array.

The insensitivity of nanotube diameter toward the external adsorption capacity is evident from the isotherms, $q^{s}_{sim,D}(P/P_0)$, plotted in Figure 4. The isotherms follow similar trends for all nanotube sizes with minimal but perceptible adsorption until $P/P_0 \approx 10^{-3}$ (<10% of the monolayer coverage value). The adsorption capacities of all arrays exhibit only small differences with respect to the tube diameter. At relative pressures lower than $P/P_0 = 10^{-5}$, wider nanotubes have higher external adsorption capacities, which would favor their use in environmental applications of sensors and removal of pollutant gases in very low concentrations (ppb and ppm levels). For bulk

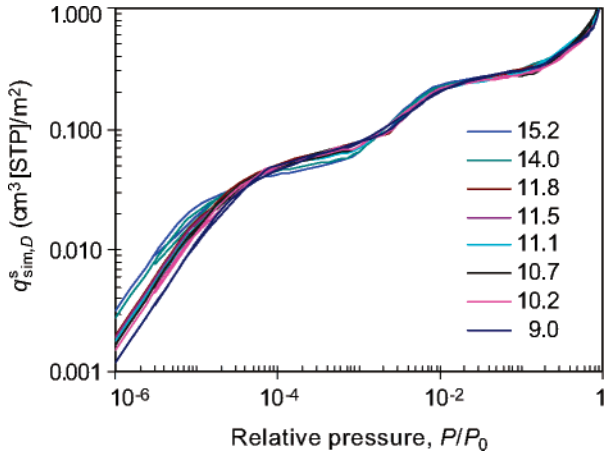

Figure 4. GCMC nitrogen adsorption isotherms at 77 K on the external surface of homogenous bundles of nanotubes with diameters identical to those found in samples EA95 and CVD80. Notice that due to the log scale on the *y*-axis it appears that at low concentrations wider nanotubes have significantly higher adsorption capacities than small diameter nanotubes.

separation and gas storage applications, however, it is reasonable to say that adsorption on the external surface of the bundle is insensitive to nanotube diameter. In this case, q^s_{sim} can be safely replaced by the external isotherm $q^s_{sim,\tilde{D}}$ for a homogeneous bundle with a reference tube diameter, $\tilde{D}$, selected from within the range of the experimental tube diameter distribution. The most obvious choice for $\tilde{D}$ is the average diameter, $\langle D \rangle$, though the value corresponding to the strongest peak of the tube diameter distribution is also an acceptable choice.

The external surface area, S_p in eq 9, of each sample was determined by plotting the total experimental adsorption capacity of the sample, q_{exp} (cm³ [STP]/g), versus the simulated amount adsorbed on the external surface of the bundle, q^s_{sim} (cm³ [STP]/m²) in eq 10, at the same relative pressure (Figure 5). Each plot can be interpreted as being comprised of two parts, with the first part showing a steep rise and the second part nearly following a straight line. The first portion of the curve indicates that the experimental adsorption capacity surpasses the simulated values, which means that the total adsorption in the sample is much higher than the external adsorption. The second part of the curve implies that the experimental adsorption capacity is linearly proportional to the simulated external adsorption capacity or, in other words, that the majority of adsorption in the sample is occurring on the external surface of the bundles. The slope of the linear part of the curve, thus, represents the total external surface area of the bundles in the sample, because in the corresponding P/P_0 range $q^i_{sim}(P/P_0)$ in eq 9 is constant and equal to its saturation value, $q^\mu_{sim} \equiv q^i_{sim}(1)$.

Additionally, the linear part of the curve when extrapolated to the simulated adsorption axis gives a positive intercept which is equivalent to the micropore volume of the sample, q^μ_{sim}. This volume is comprised of the intratube space of those nanotubes which are open-ended and the interstitial channels between sufficiently large nanotubes where adsorption can occur. Furthermore, the relative pressure at the point of inflection in the curve (i.e., the point where the two parts of the curve cross) is indicative of the maximum pressure above which the internal volume of nanotubes is filled.

The total external surface area of the bundles, S_p, and the micropore volume, q^μ_{sim}, of each sample, as calculated by the method described above, are presented in Figure

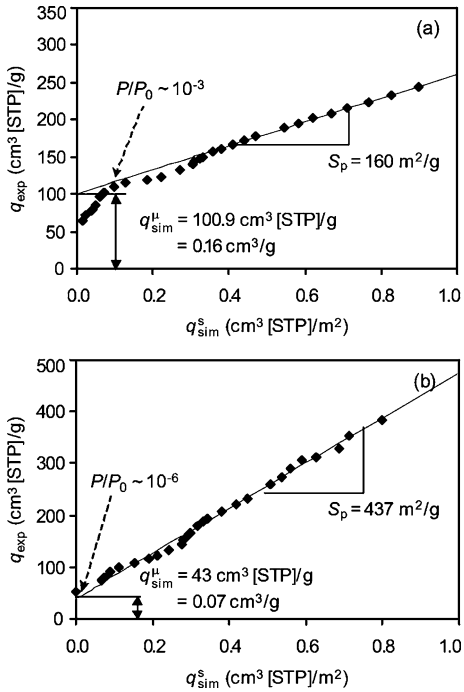

Figure 5. Total experimental adsorption capacity vs simulated external adsorption capacity for samples (a) EA95 and (b) CVD80. The slope and intercept of the straight line fitting the linear portion of the data give, respectively, the external surface area and micropore volume of the sample.

5. The two plots show that the internal adsorption volume of sample CVD80 is filled at pressures much lower than those for sample EA95. This is in agreement with the tube diameter distributions determined by Raman spectroscopy, which indicate that sample CVD80 has smaller tube diameters than sample EA95. The total external surface area of sample CVD80 (437 m²/g) is larger than that of sample EA95 (160 m²/g), which indicates the presence of thinner bundles in sample CVD80. The micropore volume (Table 3) determined by the *t*-plot method[31] incorporated in the Micromeritics ASAP software is in excellent agreement with that obtained by our procedure for both samples. The total external surface areas given by the two procedures are, however, different, with noticeable differences for sample CVD80. The discrepancy is due mainly to the use of nonporous carbon as the reference adsorbent for the standard isotherm of the *t*-plot method, which is clearly inadequate for a structured porous adsorbent such as a nanotube bundle.[32] Another contribution to this discrepancy is that the definition of external surface area adopted in this work (see Figure 1b) is likely to be incompatible with that assumed by the software implementation of the *t*-plot method.

3.2. Internal Adsorption. Simulations of nitrogen adsorption inside the nanotube array (henceforth, referred to as internal adsorption) reveal that the interstitial channels between neighboring nanotubes are generally not preferred for adsorption. However, single file adsorption of nitrogen molecules in these sites is observed for arrays of 15.2 Å wide nanotubes (Figure 6), although significant amounts are observed only at comparatively high relative pressures ($P/P_0 > 10^{-4}$). The effective width of the interstitial channel depends on the size of the neighboring nanotubes, and as a result, for large diameter nanotubes, it can be wide enough to accommodate a row

(31) Lippens, B. C.; de Boer, J. H. *J. Catal.* **1965**, *4*, 139.
(32) Ohba, T.; Kaneko, K. *J. Phys. Chem. B* **2002**, *106*, 7171.

Table 3. Surface Area and Pore Volumes of Samples EA95 and CVD80 as Determined from Simulations and Experiments of Nitrogen Adsorption at 77 K[a]

	simulation values								experimental values[d]			
	maximum[b]				adjusted[c]							
	surface area		pore volume		surface area		pore volume		surface area		pore volume	
sample	T	Ex	TP[e]	μP	T	Ex	TP[e]	μP[f]	T	Ex	TP[g]	μP
EA95	1207	160	0.64	0.34	566	160	0.45	0.15	507	155	0.57	0.16
CVD80	0892	437	0.84	0.11	781	437	0.79	0.08	609	339	0.92	0.07

[a] The total BET (T) and external (Ex) surface areas are in m^2/g, and the total pore (TP) and micropore (μP) volumes are in cm^3/g. [b] All nanotubes are assumed to be open-ended. [c] $\alpha = 0.45$ for EA95, and $\alpha = 0.60$ for CVD80. [d] Source: ref 23. The experimental micropore volumes presented here were determined by the standard *t*-plot method incorporated in the Micromeritics ASAP software. [e] Calculated at $P/P_0 = 0.90$. [f] Comparable to the q^{μ}_{sim} values in Figure 5. [g] Calculated at $P/P_0 = 0.99$.

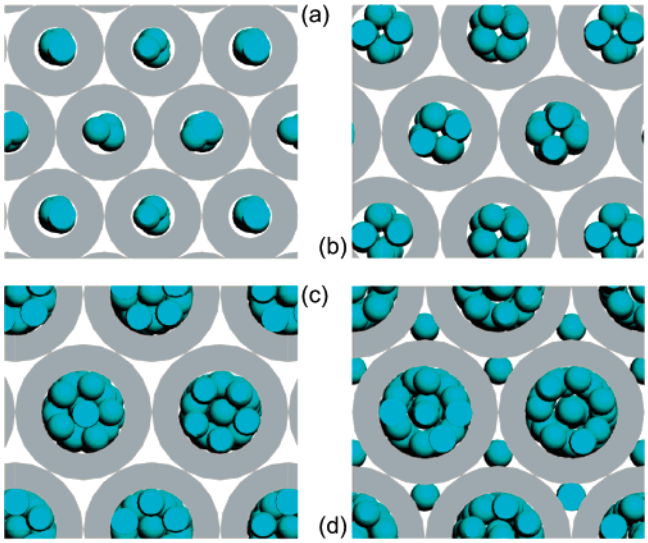

Figure 6. Snapshots of the simulation box for nitrogen adsorption at 77 K and $P/P_0 \approx 0.9$ inside SWNT bundles of tube diameter (a) 9.0 Å, (b) 11.5 Å, (c) 14.0 Å, and (d) 15.2 Å.

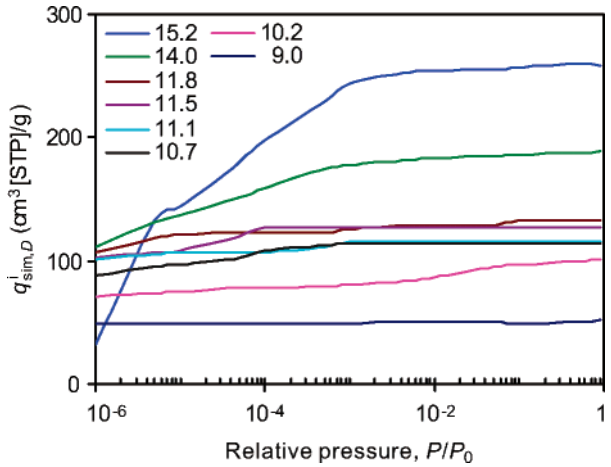

Figure 7. Simulated amount of nitrogen adsorbed at 77 K inside homogenous bundles of nanotubes with diameters identical to those found in samples EA95 and CVD80.

of nitrogen molecules. This discussion, however, is less important, as actual nanotube bundles are heterogeneous with interstitial channels of various sizes, some of which can be large enough to have unrestricted adsorption.[22]

The internal adsorption isotherms, $q^{i}_{sim,D}(P/P_0)$, of nanotube arrays indicate that, as the nanotube size is increased from 9.0 to 15.2 Å, higher relative pressures are needed to saturate the bundle (Figure 7). Arrays of 9.0 Å nanotubes are nearly saturated at nitrogen pressures as low as $P/P_0 = 10^{-6}$, whereas those of 15.2 Å wide nanotubes saturate below $P/P_0 = 10^{-3}$. Also, the adsorption capacity of a 15.2 Å nanotube array (260 cm^3 [STP]/g) is more than 5 times that of a 9.0 Å nanotube array (52 cm^3 [STP]/g). Thus, SWNT samples containing wide nanotubes have a large micropore volume that saturates at relatively high nitrogen pressure.

3.3. Total Adsorption. The total adsorption capacity of each sample, as determined from simulations, was calculated by summing its internal and external adsorption contributions according to eq 9. The corresponding adsorption isotherms are plotted in Figure 8. The simulated isotherms were used to calculate the total surface area and the total pore volume of the samples. The micropore volume of the samples was determined from the maximum internal adsorption (eq 9). These values are listed in Table 3.

For sample EA95, $P/P_0 \approx 10^{-3}$ appears to be a critical point in the isotherm as the internal adsorption saturates at that relative pressure and the external adsorption becomes significant. For sample CVD80, however, the internal adsorption is almost saturated at a much lower pressure ($P/P_0 \approx 10^{-6}$) and the external adsorption is also significant at a much lower P/P_0 value ($\approx 10^{-5}$). These results are in compliance with the results presented in Figure 5. Also, at any given P/P_0 value, the internal adsorption is much higher and the external adsorption is much lower in sample EA95 than in sample CVD80. Additionally, the total BET surface area and micropore volume of sample EA95 (1207 m^2/g and 0.34 cm^3/g) are higher than those for sample CVD80 (892 m^2/g and 0.11 cm^3/g) (cf. Table 3). Thus, it can be concluded that samples containing large diameter nanotubes (EA95) are more suitable for gas separation and storage than those containing small nanotubes (CVD80), unless there is particular interest in exploiting the potential sieving properties of thin nanotubes.

The comparison of simulated isotherms of both SWNT samples with experimental isotherms reveals two important points (Figure 8). First, the shape of the simulated isotherm is similar to that of the experimental isotherm, which suggests that the methodology of calculating the adsorption isotherm (as a combination of external and internal adsorption in homogeneous bundles) is most likely correct. Second, the adsorption capacity and total and micropore volumes for the simulated isotherm are much higher than the corresponding experimental values (Table 3), which suggests that the simulated values are highly idealized.

In fact, the calculations were carried out with the implicit assumption that all nanotubes are open and thus contribute to the internal and total adsorption. Consequently, the simulated isotherms plotted in Figure 8, and the corresponding values of pore volume (Table 3), are the maximum achievable values for each sample. In reality, however, only a few nanotubes are open. To take this into account, a factor describing the fraction of open-ended

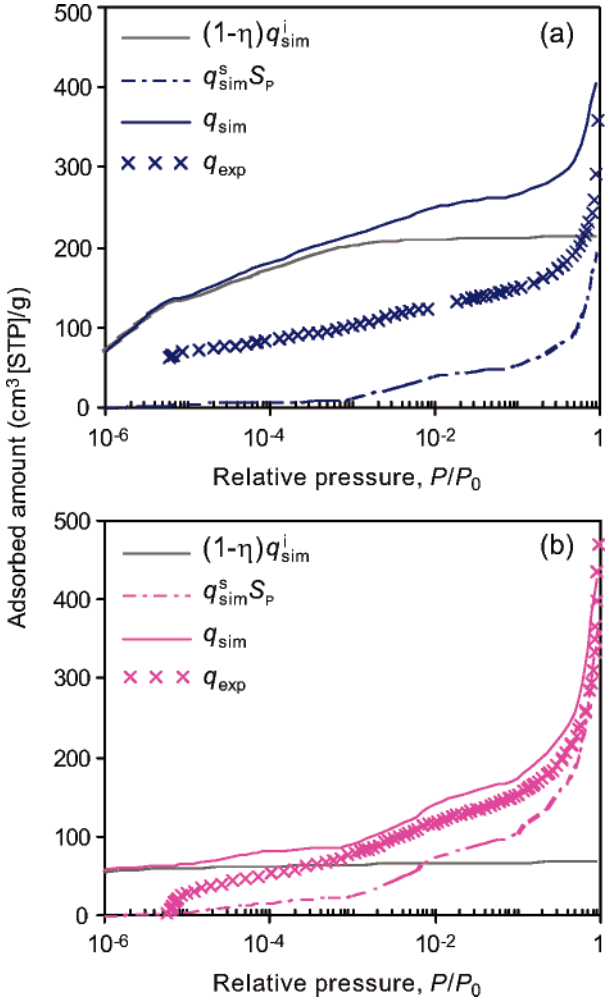

Figure 8. Nitrogen adsorption capacity of SWNT samples (a) EA95 and (b) CVD80 at 77 K, as predicted by molecular simulation, q_{sim}, and its comparison with the experimental data, q_{exp}. $S_p q^s_{sim}$ and $(1-\eta)q^i_{sim}$ are, respectively, the external and internal contributions to the total adsorption capacity, q_{sim}. Notice that, due to a larger total external surface area, the external adsorption capacity of sample CVD80 is higher than that of sample EA95.

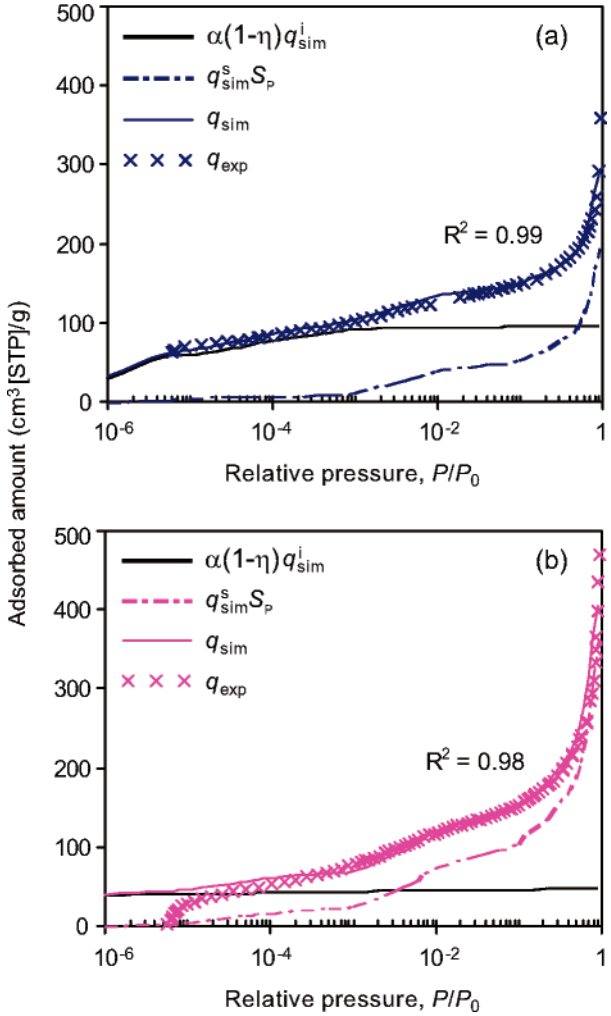

Figure 9. Nitrogen adsorption capacity of SWNT samples (a) EA95 and (b) CVD80 at 77 K, as predicted by molecular simulation, q_{sim}, and its comparison with the experimental data, q_{exp}, by assuming that $100\alpha_{EA95} = 45\%$ and $100\alpha_{CVD80} = 60\%$ of the nanotubes are open-ended. $S_p q^s_{sim}$ and $\alpha(1-\eta)q^i_{sim}$ are, respectively, the external and internal contributions to the total adsorption capacity, q_{sim}. Notice the near perfect replication of the experimental isotherms.

nanotubes should be incorporated into the calculations. This procedure should alter the internal adsorption capacity of the bundles without affecting the external adsorption, as adsorption outside the bundles occurs for both open- and close-ended nanotubes. Thus, the internal contribution to total adsorption in eq 9 should be replaced by

$$(1-\eta)\sum_{D=\text{sample}} \alpha_D w_D q^i_{sim,D}(P/P_0) \qquad (11)$$

where α_D is the fraction of open-ended nanotubes of diameter D. If it is further assumed that a process that opens a nanotube (acidic purification, heating in air, etc.) is equally effective for all nanotube sizes, then eq 11 can be further simplified as

$$\alpha(1-\eta)\sum_{D=\text{sample}} w_D q^i_{sim,D}(P/P_0) \qquad (12)$$

where the subscript in α_D is dropped to indicate that it is independent of tube diameter. It should be noted that the absolute weight percent of open-ended nanotubes, however, is still different for different nanotube sizes, in accordance with their relative amount in the sample (Table 1). Note that, to simplify the analysis, in eq 12, α also scales the interstitial volume; this introduces a negligible error into our calculations, since interstitial adsorption is zero for all arrays except those comprising 15.2 Å nanotubes. The final expression for total adsorption is, thus,

$$q_{sim}(P/P_0) = S_p q^s_{sim}(P/P_0) + \alpha(1-\eta)q^i_{sim}(P/P_0) \qquad (13)$$

The parameter α can be determined by trial and error to yield an isotherm that fits the experimental isotherm. Alternately, α can also be calculated as the ratio of the experimental micropore volume to the maximum simulated micropore volume, q^μ_{sim},

$$\alpha = \frac{\text{experimental micropore volume}}{\text{maximum simulated micropore volume}} \qquad (14)$$

Adjusting α to 0.45 and 0.60 for samples EA95 and CVD80, respectively, results in a nearly perfect fit between simulated and experimental isotherms (Figure 9). Also, the BET surface area and the micropore volume of sample

EA95 closely agree with the experimental values (Table 3). The micropore volume is also comparable to the q^{μ}_{sim} value, as calculated in Figure 5. Sample CVD80, however, does not exhibit a perfect closure between simulated and experimental values at very low pressures, which is believed to be due to relatively large quantities of impurities present in the sample or too incorrect measurements at these very low pressures. Notice that the total pore volume, estimated from eq 13 at $P/P_0 = 0.9$, is smaller than the experimental value because the mesoporosity of the void space between bundles is not taken into account in our analysis. Overall, it can be said that samples EA95 and CVD80 contain 45 and 60% open-ended nanotubes, respectively.

4. Summary and Conclusions

A structural characterization procedure for SWNT samples, combining molecular simulation, Raman spectroscopy, and standard nitrogen adsorption, has been described. GCMC molecular simulations were performed to determine the nitrogen adsorption capacity on the external and internal adsorption sites of homogeneous arrays of SWNTs for the diameters determined from the Raman analysis of the sample. Adsorption on the grooves present on the periphery of a nanotube bundle was observed at vapor concentrations as low as $P/P_0 = 10^{-6}$, with the total external adsorption being weakly dependent on nanotube size, except at very low relative pressures. The internal adsorption isotherms of nanotube arrays indicate that adsorption in the interstitial channels between nanotubes can occur in homogeneous arrays of wide nanotubes ($D > 15$ Å) and that both the amount of nitrogen adsorbed and the relative pressure at which the bundles are saturated increase with increasing nanotube size. Comparison with the standard nitrogen adsorption experiments suggests that considering only a fraction $0 < \alpha < 1$ of the total adsorption inside the nanotubes results in a near perfect fit between simulated and experimental values for both samples. The parameter α is interpreted as the fraction of open-ended nanotubes present in the sample. This analysis shows that samples EA95 and CVD80, which were experimentally studied in a previous work,[23] contain only 45 and 60% open-ended nanotubes, respectively. Our procedure allows extrapolation of adsorption properties to conditions in which all nanotubes in the sample are open-ended. Under those ideal conditions, the BET surface area of samples EA95 and CVD80 can be increased from 507 and 609 m^2/g, respectively, to a maximum of 1207 and 892 m^2/g.

Acknowledgment. The Graduate College and the European Union Center of the University of Illinois and NATO (SfP Project No. 977984) are highly appreciated for providing necessary travel grants to accomplish this work.

LA047662C